Targeted deletions of complement lectin pathway genes improve outcome in traumatic brain injury

Domenico Mercurio
Istituto di Ricerche Farmacologiche Mario Negri IRCCS https://orcid.org/0000-0001-5101-7222
Marco Oggioni
Istituto di Ricerche Farmacologiche Mario Negri IRCCS
Stefano Fumagalli
IRCCS-Istituto di Ricerche Farmacologiche Mario Negri
Nicholas Lynch
University of Cambridge https://orcid.org/0000-0003-3803-3329
Silke Roscher
University of Leicester
Denise Minuta
Istituto di Ricerche Farmacologiche Mario Negri IRCCS
Carlo Perego
Mario Negri Institute for Pharmacological Research
Stefania Ippati
Istituto di Ricerche Farmacologiche Mario Negri IRCCS
Russell Wallis
University of Leicester
Wilhelm Schwaeble
University of Cambridge
Maria-Grazia De Simoni (desimoni@marionegri.it)
Mario Negri Institute for Pharmacological Research

Article

Keywords: Traumatic brain injury, neuroinflammation, lectin activation pathway of complement, MBL-associated serine protease

Posted Date: July 17th, 2020

DOI: https://doi.org/10.21203/rs.3.rs-39050/v1

Main Manuscript for

Targeted deletions of complement lectin pathway genes improve outcome in traumatic brain injury

Mercurio D.[1], Oggioni M.[1], Fumagalli S.[1], Lynch N.J[1,3], Roscher S. [2] , Minuta D.[1#], Perego C. [1], Ippati S. [1##], Wallis R. [2], Schwaeble W. [3] and De Simoni M.G.[1*]

[1]Department of Neuroscience, Istituto di Ricerche Farmacologiche Mario Negri IRCCS, via Mario Negri 2, 20156, Milan, Italy;

[2]Department of Respiratory Sciences, University of Leicester, University Road, LE1 7RH, Leicester, UK;

[3]Department of Veterinary Medicine, University of Cambridge, Madingley Road, CB3 0ES, Cambridge, UK

[#] Present address: San Raffaele Telethon Institute for Gene Therapy (SR-Tiget), San Raffaele Hospital, Milan 20132, Italy.

[##] Present address: National Research Council (CNR), Institute of Neuroscience, Milan 20129, Italy

***Corresponding author**:

Maria-Grazia De Simoni,

Istituto di Ricerche Farmacologiche Mario Negri IRCCS

via Mario Negri 2, Milan 20156, Italy.

Email: desimoni@marionegri.it

Keywords

Traumatic brain injury, neuroinflammation, lectin activation pathway of complement, MBL-associated serine protease

Abstract

The complement system is believed to contribute to inflammation in acute brain injury. This work defines the neurobehavioral response to traumatic brain injury (TBI) modeled by controlled cortical impact in wild-type mice and in mice carrying gene-targeted deficiencies of individual components of the lectin pathway of complement activation to identify the key components contributing to pathology. Targeted gene deletions include: the recognition subcomponents ficolin-A, CL-11, MBL-C and MBL-A, both individually and combined, and the serine proteases MASP-1, MASP-2 and MASP-3. Our results demonstrate that MASP-2 deficiency brings the highest protective phenotype, countering long-term neuroinflammatory injury following TBI, as shown by reduced neuronal deficits and neuronal cell loss compared to wild-type mice. This study highlights MASP-2 as a promising pharmacological target in patients suffering from TBI, a leading cause of death and disability.

Main Text

Introduction

Traumatic brain injury (TBI) is associated with a primary biomechanical injury that can involve contusion and laceration, diffuse axonal injury, brain swelling and intracranial haemorrhage[1–3] followed by a secondary injury, which is caused by the activation of several molecular and cellular cascades contributing to brain damage and its development over time[4–6]. Secondary insult response typically includes blood-brain barrier (BBB) breakdown, oxidative stress, glutamate

excitotoxicity, and neuroinflammation[7–9]. Since the secondary damage evolves days after the impact, there are windows of opportunity for pharmacological therapeutic interventions.

The complement system, an important component of the innate and adaptive immune response, is a major coordinator of post-traumatic neuroinflammation and secondary neuropathology after TBI[10–14]. Even in absence of infection (which can be an additional complication following TBI) the complement system can be activated by endogenous danger signals called damage-associated molecular patterns (DAMPs)[15]. Depending on the signals, complement activation may occur through three different pathways, the classical, the alternative and the lectin pathway (LP), each composed of specific initiators and effector enzymes. Carbohydrate structures or acetylated proteins exposed on the surface of damaged cells, including apoptotic or necrotic cells and stressed endothelium[16], are typical DAMPs recognized by the LP. The LP is initiated by recognition molecules such as mannose-binding lectin (MBL, rodents have two isoforms, MBL-A and MBL-C), collectin-11 (CL-11) and ficolins (in humans: ficolin-1, 2 and 3; in rodents: ficolin-A and ficolin-B), acting as soluble receptors. They circulate in normal conditions complexed with MBL-associated serine proteases (MASPs). In both humans and mice, MASP-1 and MASP-3 are alternative splicing variants encoded by a single structural *MASP1* gene, while MASP-2 is encoded by a separate *MASP2* gene located on a different chromosome[15,17]. LP activation complexes initiate complement activation through two independently operating mechanisms: 1) through MASP-2 as the only enzyme that is essential to drive the LP through its ability to form C3 convertase complex, C4b2a and 2) MASP-3 that enables the alternative activation pathway of complement by converting the essential alternative pathway enzyme Factor D from its zymogen form into its enzymatically active form[18,19]. Cleavage of C3 by the C3 convertase initiates all downstream complement activation processes and leads to the generation of C3b (the main opsonin of the complement system) and C3a, a complement chemoattractant and anaphylatoxin. C3b can also bind to complement factor B, a serum zymogen which can only be converted when bound to C3b as C3bB complex by another serum protease called Factor D to form the C3 convertase of the alternative pathway C3bBb. A positive feedback loop is generated through the

ability of the cleavage product C3b to form further C3 converting C3bBb complexes which contributes to an amplification of complement activation and constitutes the alternative activation pathway of complement. C3b is also a constituent of the C5 cleaving enzyme complexes, ie. C3bBb (C3b)n (for the alternative pathway and C4bC2a(C3b)n for the CP and the LP). The cleavage of C5 releases the complement anaphylatoxin C5a and initiates the formation of the membrane attack complex (C5b-9)[20]. As a result of the full cascade activation, local brain inflammation is enhanced contributing to the pathophysiological mechanisms underlining brain injury.

There is a strong body of evidence showing that LP activation critically contributes to disease severity in the pathogenesis of brain ischemic injury. Genetic deletion of LP sub-components (MBL or MASP-2)[21–23] or their pharmacological targeting[21,22] are protective in experimental models of brain ischemia. In addition to a key role of the enzyme MASP-2, the recognition subcomponent MBL itself was shown to possess direct activity, driving platelet-dependent inflammation and vascular damage following ischemic injury independent of LP activation[16,24]. Of note, TBI shares blood perfusion deficits and metabolic derangements with ischemic injury[25], thus suggesting that similar mechanisms might be involved in the traumatic pericore tissue, an area subjected to post-injury hypoxia [26].

In human TBI contusions, the LP recognition molecules (MBL, ficolin-1, ficolin-2, ficolin-3 and CL-11/CL-10) and the enzymes MASP-2 and MASP-3 have been found deposited inside and outside the cerebral vessels. Importantly, MBL, ficolin-2 and ficolin-3 levels are elevated in the brains of TBI compared to non-TBI patients and perivascular MASP-2 deposition increase with injury severity [26]. These results demonstrate the involvement of the LP in TBI pathology, although the specific recognition molecules or enzymes which more prominently contribute to the TBI *sequelae* remain elusive. The comparative analysis shown here, identifies the most effective targets for therapeutic interventions, aiming to reduce post traumatic inflammatory responses, brain tissue loss and to ameliorate cognitive functions following TBI. In this study, we compared the neurobehavioral outcome and health score up to 4 weeks after TBI of wild-type (WT) mice and of

mice knocked-out for MASP-2 (*Masp2*$^{-/-}$), ficolin-A (*Fcna*$^{-/-}$), CL-11 (*Colec11*$^{-/-}$), MASP-1/3 (*Masp1*$^{-/-}$), MBL-C (*Mbl2*$^{-/-}$), MBL-A (*Mbl1*$^{-/-}$) or MBL$^{-/-}$ (*Mbl1*$^{-/-}$/ *Mbl2*$^{-/-}$). Our results demonstrate that MASP-2 deficiency brings the highest protective phenotype, countering long-term neuroinflammatory injury following TBI, as shown by reduced neuronal deficits and neuronal cell loss compared to wild-type mice. MBL$^{-/-}$ and FCN-A$^{-/-}$ mice were also significantly protected and presented good outcome scores, indicating that these molecules might be relevant initiators of the inflammatory response to TBI.

Results

MASP-2$^{-/-}$ mice showed the best outcome after TBI with reduced sensorimotor deficits.

This study was conducted according to the plans depicted in Fig 1A. Wild-type (WT) or KO mice (including: MASP-2$^{-/-}$, FCN-A$^{-/-}$, CL-11$^{-/-}$, MBL-C$^{-/-}$, MASP-1/3$^{-/-}$ and MBL-A$^{-/-}$) were subjected to TBI or sham injury. Sensorimotor deficits were assessed weekly for 4 weeks by neuroscore and beam walk tests. The data related to the sensorimotor performance are summarized in Table 1. The health score and odds ratio data for MBL$^{-/-}$ mice were calculated using previously published data from our lab[27]. To obtain a comparative evaluation of the transgenic lines, a health score based on the outcome of the two sensorimotor tests was calculated. Mice were rated from 1 (bad outcome) to 4 (good outcome, Fig 2A).

MASP-2$^{-/-}$ was the most protective genotype, showing a positive association with a good outcome (odds ratio 56.3 [95% CI, 1.9-1655], p = 0.002). MBL$^{-/-}$ and FCN-A$^{-/-}$ mice were also significantly protected, showing a positive association with a good outcome, but to a lesser extent than MASP-2$^{-/-}$ (p = 0.0017 and p=0.0386; odds ratio 36 [2.7 – 476.3] and 9.1 [0.9 – 92.4], respectively). CL-11$^{-/-}$ and MBL-C$^{-/-}$ genotypes showed a weaker, non-significant association with a good outcome (p = 0.0566 and p = 0.5582 respectively), whereas MASP-1/3$^{-/-}$ and MBL-A$^{-/-}$ mice were not protected (p = 0.5570 and p = 0.527 respectively, Fig 2B).

MASP-2$^{-/-}$ mice had higher neuronal density than WT mice after TBI.

Based on the outcome data, we focused on the MASP-2$^{-/-}$ genotype and assessed the lesion size at 6 weeks (neuronal density, GFAP and CD11b immunostaining) and the degree of local brain inflammation at 30 min (presence of MBL-C in the brain and residual LP activity in plasma) (Fig 1B). At 6 weeks post injury, we observed an extensive macroscopic area of cortical tissue loss, extending rostrocaudally from bregma + 0.4 to - 3.6 mm, both in WT and MASP-2$^{-/-}$ injured mice, without differences between the two genotypes (17.2 ± 1.6 vs 18.6 ± 1.0 mm^3 ± SEM Fig 3A-C). We then assessed the neuronal density in a cortical region traced at a distance of 350 μm from the contusion edge (Fig 3D, E) and in the corresponding contralateral hemisphere. MASP-2$^{-/-}$ mice had higher neuronal density than WT mice at six weeks after TBI (31.5%, $p < 0.05$, Fig 3G), indicating that the absence of MASP-2 functional activity was significantly protective against neuronal death after TBI.

MASP-2$^{-/-}$ mice did not show different astrogliosis and microglial activation after TBI.

At six weeks after TBI, we measured astrogliosis and microglial activation quantifying the GFAP and CD11b immunopositive area at the edge of the contusion area. WT and MASP-2$^{-/-}$ injured mice showed comparable astrogliosis (17.8 ± 2.1 vs 16.5 ± 2.3 staining % area ± SEM) and microglial activation (8.5 ± 1.8 vs 8.7 ± 1.7 staining % area ± SEM) when assessed as the total stained area (Fig 4A, B). Since microglia morphology is indicative of the state of microglial activation, we subsequently analysed microglial cell shape descriptors[25]. Our analysis revealed that the proinflammatory morphology of microglia persists for as long as 6 weeks after TBI. Increased size (area, perimeter and Feret diameter) and higher ramified morphology (lower circularity) were observed in the ipsilateral region compared to the contralateral hemisphere ($p < 0.01$). However, no differences in microglial morphology were observed when comparing WT and MASP-2$^{-/-}$ mice (Fig 4C).

MASP-2$^{-/-}$ mice had impaired Lectin Pathway activation and normal MBL-C deposition.

Since MBL-C deposition can be detected in the brain after TBI[27], we measured the relative amount of MBL-C deposits in WT and MASP-2$^{-/-}$ injured mice 30 minutes after injury (Fig 5A). We observed an increased deposition of MBL-C in TBI mice (compared to sham), regardless of the genotype (WT vs MASP-2$^{-/-}$ 1.30 (± 0.08) x10^{11} vs 1.10 (± 0.12) x10^{11} fluorescence integrated density ± SEM Fig 5B) indicating that the absence of MASP-2 did not affect the deposition of MBL-C. We then tested LP functional activity in mouse plasma using a functional *in vitro* assay[18] on mannan-coated plates, which measures LP activation through MBL (92.6 ± 15.2 vs 7.3 ± 1.7 optical density ± SEM)[28]. The absence of C4b deposition shows that MBL driven LP activation does not occur in MASP-2$^{-/-}$ TBI mice, indicating that not even residual activation of the LP is occurring in MASP-2$^{-/-}$ mice following TBI (Fig 5C)

Discussion

This study compares the long-term outcome after experimental TBI in mouse lines with targeted deficiencies of the LP-specific components, namely the recognition molecules ficolin-A, CL-11, MBL-C and MBL-A (both individually and combined) and the serine-proteases MASP-2, MASP-1 and MASP-3. To obtain a comparative outcome analysis, we developed a health score based on the neuroscore and beam walk test, two behavioural analyses evaluating sensorimotor deficits, over 4 weeks of observation. We found that MASP-2$^{-/-}$, MBL$^{-/-}$ and FCN-A$^{-/-}$ mice had lower neurological deficits after TBI, indicating that these LP components are actively involved in driving the traumatic lesion and identifies them as possible pharmacological targets to reduce post-traumatic loss of functional activity and to improve recovery and clinical outcome.

MASP-2$^{-/-}$ mice had the strongest reduction in sensorimotor deficits after TBI, which is in line with the key role of this enzyme in driving LP dependent complement activation. Of note, 6 weeks after injury, MASP-2$^{-/-}$ TBI mice had higher neuronal density in the ipsilateral cortex compared to WT TBI mice, an important result given the severity of the TBI model used which has a major

184 impact on neuronal viability and leads to major brain tissue loss. This is similar to what is
185 observed in patients suffering from severe injury[26].
186 Our data underline the importance of the LP in TBI pathophysiology and identify MASP-2 as a
187 key enzyme. Interestingly, neither of the other LP-associated enzymes, i.e. MASP-1 or MASP-3
188 appear to be involved in the posttraumatic loss of CNS functions following TBI, since MASP-1/3$^{-/-}$
189 mice suffered from a similar degree of sensorimotor deficits than their WT controls. While it is
190 accepted that only MASP-2 can generate the C3 convertase of the LP (C4bC2a) through its
191 ability to cleave both C4 and C2[29,30], MASP-1 can support MASP-2 functional activity by cleaving
192 C2 and enhance the conversion of zymogen MASP-2 into its enzymatically active form[31,32].
193 It has been postulated that MASP-1 is an essential activator of MASP-2 [33] based on *in vitro*
194 experiments using MASP-1/3 or MASP-1 deficient sera or sera treated with MASP-1 specific
195 inhibitors. However, in *in vivo* models of MASP-2 dependent pathophysiology such as ischemia
196 reperfusion injury and TBI reported here, the requirement for MASP-1 to activate MASP-2
197 appears to be negligible since the absence of MASP-1 (or MASP-3) does not protect from MASP-
198 2 dependent tissue injury. MASP-1 facilitates the conversion of zymogen MASP-2 into its
199 enzymatically active form, most likely because the relatively low abundance of MASP-2 compared
200 to MASP-1 limits LP-specific trans-activation events[34,35]. In an experimental model of ischemic
201 stroke, we reported that combined deficiency of MASP-1 and MASP-3 did not affect the ischemic
202 outcome, while that of MASP-2 was protective[22]. Therefore, we hypothesized that, ischemic brain
203 injury involved a MASP-2 dependent pathophysiological process, thus underlining that MASP-1 is
204 not an essential activator of MASP-2. Consistent with this conclusion is our present observation
205 that the total absence of LP-mediated complement activation in MASP-2$^{-/-}$ mice is protecting from
206 post-traumatic injury, while MASP-1/3 double deficient mice show no degree of protection. In this
207 context, it is important to keep in mind that MASP-2 can also cleave C3 directly through a C4 and
208 C2 independent bypass activation of native C3[36].
209 Our study shows that MBL$^{-/-}$ and FCN-A$^{-/-}$ mice were significantly associated with a good outcome
210 scores indicating that they may be the relevant initiator molecules. In line with this, we have

previously shown the effectiveness of targeting MBL in TBI mice by inhibiting MBL with Polyman9, a polymannosylated compound binding to its carbohydrate recognition domain, attenuating sensorimotor deficits up to four weeks after TBI[27,37]. As for ficolin-A, the mouse orthologue of human ficolin-2, no data are available on its role in the context of brain injury. In TBI patients ficolin-2 has been found in the peri-contusional brain area at significantly higher levels than in the brain from control patients[26]. Its role in TBI has to be further investigated.

A common feature of the initiators of the lectin complement pathway is their ability to interact with MASP-2 to trigger the activation of the LP. Thus, MASP-2 inhibition should be a more effective target than one of the five LP initiators. The data obtained in this work supports this notion, as MASP-2 deficiency provides better protection against TBI damage than that of a specific initiator. However, as previously reported in models of ischemia/reperfusion injury, recognition molecules can have detrimental effects independently from the LP cascade activation[16,38]. In particular, MBL itself has been shown to promote vascular injury on endothelial cells having undergone hypoxic stimulus by direct action - including structural damage to the endothelial cell cytoskeleton - without requiring LP activation[16]. Consistent with this finding, genetic deletion of MBL or its pharmacological inhibition were sufficient to obtain significant protection in experimental models of ischemic stroke, where vascular dysfunction is critical [21,24,39]. The fact that in experimental TBI, MBL depletion provided a lower degree of protection than MASP-2 depletion may suggest that MBL complement-independent vascular effects are less important for TBI pathophysiology. In line with this suggestion, the presence of MBL within the TBI-injured area was not different in WT and MASP-2$^{-/-}$ mice, supporting the hypothesis that LP-independent detrimental effects of MBL have a limited contribution to TBI sequelae. Moreover, the presence of MBL in the lesion core area was observed mostly extravascularly, therefore implying that MBL-driven vascular effects may be marginal, at variance with what happens in ischemic injury.

In our previous work on the role of MASP-2 in ischemia/reperfusion injury, we reported that microglia within the ischemic areas presented morphological features typical of their anti-inflammatory activity, as opposed to the hypertrophic microglial morphology associated with the

phagocytic activity and pro-inflammatory state present in ischemic WT brains[22]. Here, we studied microglia in the cortical brain area close to the contusion edge. Six weeks post-injury microglia was still activated, showing increased size and ramifications in ipsi- compared to contra-lateral side. Notably, chronic microglia activation may contribute to specific behavioural deficits, like sickness behaviour in mice, corresponding to depressive behaviours seen in TBI patients months after injury[40,41]. However, no difference in microglia morphology was detected between the two genotypes suggesting that the LP does not play an important role in the chronic activation of microglia after TBI.

The results presented here, obtained in experimental TBI, pointing to MASP-2 as a key enzyme in TBI pathology, are in line with what observed in TBI patients. Namely, we previously reported that: 1) the complement system is fully activated down to the level of the formation of the terminal complement complex; 2) the lectin pathway components are persistently present, up to five days post-TBI; and 3) MASP-2 in the brain is significantly increased and associated with TBI severity, indicated by abnormal pupil reactivity and traumatic subarachnoid haemorrhage[26]. Moreover others reported that increased circulating levels of MASP-2 are associated with a poor outcome at 90 days after injury[42].

It should not be excluded that other pathways of complement system may have a role in propagating chronic post-TBI pathology. Indeed, we also reported an increased presence of MASP-3 in the brains of TBI patients compared to control patients[26], supporting a role of the alternative pathway in TBI. Indeed its pharmacological inhibition provided significant improvements in histological, and functional recovery in an experimental model of TBI[43].

In conclusion, this study confirms that the LP critically contributes to the post-traumatic inflammatory pathology following TBI and shows that the highest degree of protection is achieved through the absence of the LP key enzyme MASP-2, underlying the therapeutic utility of MASP-2 targeting following acute brain injury. This points to LP and MASP-2 as key pharmacological targets for TBI, thus paving the way for future development of clinical strategies. It represents a unique target: it is a single, low-abundance enzyme that is exclusively synthesized in the liver[44],

so the effectiveness of systemic MASP-2 inhibitory agents is not complicated by local biosynthesis in the brain and the limitations imposed by the blood-brain barrier. Of note, an inhibitory antibody against MASP-2 (Narsoplimab) is currently undergoing phase 3 clinical trials for the treatment of Hematopoietic Stem Cell Transplant-Associated TMA (ClinicalTrials.gov Identifier: NCT04247906), IgA Nephropathy (NCT03608033) and Atypical Hemolytic Uremic Syndrome (NCT03205995) and in a phase 2 clinical trial for the treatment of Lupus Nephritis (NCT02682407), thus making the present work potentially transferable to the clinical setting in the near future.

Methods

Mice

Procedures involving animals and their care were conducted in conformity with institutional guidelines in compliance with national and international laws and policies (prot.9F5F5.81 authorisation n° 753/2017-PR). We used male 9 week old C57BL/6 J mice weighing 22–28 g, either WT (purchased from Charles Rivers-Italy) or with targeted deletion of MASP-2, ficolin-A, CL-11, MASP-1/3 (*Masp2*$^{-/-}$, *Fcna*$^{-/-}$, *Colec11*$^{-/-}$, *Masp1*$^{-/-}$ Biomedical Services, University of Leicester) MBL-C and MBL-A, (*Mbl2*$^{-/-}$ and *Mbl1*$^{-/-}$ obtained at Mario Negri Institute by crossing MBL$^{-/-}$ mice with WT mice and selecting appropriate colony founders). The protocols and details of this report are in accordance with ARRIVE guidelines (http://www.nc3rs.org.uk/page.asp?id=1357, check list provided as supplementary file).

Experimental traumatic brain injury

Mice were anesthetized with isoflurane inhalation (induction 5%; maintenance 2%) in an N_2O/O_2 (70/30%) mixture and placed in a stereotactic frame. Mice were then subjected to craniotomy followed by induction of controlled cortical impact (CCI) brain injury as previously described[45–48]. Briefly, the injury was induced using a 3 mm diameter rigid impactor driven by a pneumatic piston

rigidly mounted at an angle of 20° from the vertical plane and applied vertically to the exposed dura mater, between bregma and lambda, over the left parieto-temporal cortex. We set an impactor velocity of 5 m/s and deformation depth 1 mm, resulting in a severe level of injury[37,49]. The craniotomy was then covered with a cranioplasty and the scalp sutured. Sham-operated mice received identical anesthesia and surgery without craniotomy and brain injury.

Behavioural tests

Neuroscore

Mice were scored from 4 (normal) to 0 (severely impaired) for each of the following: 1) forelimb function during walking on the grid and flexion response during suspension by the tail; 2) hindlimb function during walking on the grid and extension during suspension by the tail; 3) resistance to lateral right and left push. The best score is 12[37].

Beam walk

The beam walk test measures the number of foot faults of the mouse walking twice on an elevated, narrow wooden beam (5 mm wide and 100 cm long). Before each test, mice are trained in three habituation trials. Data are expressed as the sum of the number of foot faults during the two tests. The best score is 0[37].

Tissue processing

At six weeks after surgery, under deep anesthesia (Ketamine 20 mg + Medetomidine 0.2 mg), animals were transcardially perfused with 30 mL of phosphate buffer saline (PBS) 0.1 mol/L, pH 7.4, followed by 60 mL of chilled paraformaldehyde (4%) in PBS. The brains were carefully removed from the skull and post-fixed for 6 h at 4 °C, then transferred to 30% sucrose in 0.1 mol/L phosphate buffer for 24 h until equilibration. The brains were frozen by immersion in isopentane at −45 °C for 3 min before being sealed into vials and stored at −80 °C until use. Coronal brain 20 µm-thick cryosections were cut serially (from bregma +1.2 mm to bregma −4

mm) at 200 µm intervals and stained with Cresyl violet (Sigma-Aldrich) using standard histological protocols[48,50].

Contusion volume

Eight coronal section from bregma +0.6 to -4.0 mm were acquired with an Olympus BX-61 Virtual Stage microscope using a 2x objective lens, with a pixel size of 3.49 µm. Contusion volume was analysed as previously described[51].

Neuronal count

The neuronal cell count was performed at six weeks after TBI. Three 20 µm-thick coronal sections at 0.4, 1.6, and 2.8 mm posterior to bregma and stained with Cresyl violet (Sigma-Aldrich, St. Louis, MO) were selected from each mouse brain to quantify neuronal cell loss. The entire sections were acquired with an Olympus BX-61 Virtual Stage microscope using a 20x objective lens, with a pixel size of 0.346 µm. Acquisition was done over 10 µm thick stacks, with a step size of 2 µm. The different focal planes were merged into a single stack by mean intensity projection to ensure consistent focus throughout the sample. Neuronal count was performed by segmenting the cells over a cortical region proximal to the lesion and in the corresponding contralateral hemisphere and excluding the round-shaped signal sized below the area threshold of 25 mm^2 that is known to be associated with glial cells as reported previously[27]. Quantification was performed by Fiji software. Data were expressed as the total number of neurons quantified in the selected cortical region.

Microglia and astrocyte immunohistochemical analysis

Immunohistochemistry was performed on 20 µm-thick coronal sections from perfused mouse brains. The sections were incubated overnight at 4°C with primary monoclonal antibody anti-mouse glial fibrillary acid protein (GFAP, 0.5 µg/ml, Millipore, Billerica, MA, USA) or anti-rat CD11b (1.25 µg/ml, Bio rad, Hercules, CA, USA). Biotinylated secondary antibodies (7.5 µg/ml,

345 Vector Laboratories) were used. GFAP and CD11b immunopositive cells were identified by
346 reaction with 3,3 diaminobenzidine-tetrahydrochloride (DAB, Vector Laboratories, Burlingame,
347 CA, USA) as previously described[52]. Negative control studies, without the primary antibody, were
348 performed in parallel. Three 20 µm-thick coronal sections at 0.4, 1.6, and 2.8 mm posterior to
349 bregma were selected from each mouse brain for GFAP and CD11b quantification. The entire
350 sections were acquired with an Olympus BX-61 Virtual Stage microscope using a 20x objective
351 lens, with a pixel size of 0.346 µm. Acquisition was done over 10 µm thick stacks, with a step size
352 of 2 µm. The different focal planes were merged into a single stack by mean intensity projection
353 to ensure consistent focus throughout the sample. The ipsilateral cortex was analyzed over an
354 area included within a 350 µm radius from the contusion edge. Images were analyzed using Fiji
355 software. GFAP and CD11b immunostained area were expressed as positive pixels/total
356 assessed pixels and reported as the percentage of total stained area[37]. Microglia shape
357 descriptor analysis was performed on image processed through the algorithm previously
358 described[25]. Once segmented, the cells were measured for the following parameters: area,
359 perimeter, circularity, Feret's diameter (max caliper), aspect ratio and solidity. Mean single-cell
360 values for each parameter were used for statistics.
361
362 **MBL-C deposition in the brain**
363 The brain coronal sections were incubated overnight at 4°C with primary monoclonal antibody
364 anti-mouse MBL-C (1µg/ml; Hycult Biotechnology, Uden, The Netherlands) followed by a
365 secondary biotinylated antibody against rat IgG. Positive cells were stained with Tyramide
366 Cyanine 5 (Cy5, 1:300, Perkin Elmer, Milan, Italy). Cell nuclei were stained with 40-6-diamidino-2-
367 phenylindole (Hoechst, 1 mg/ml, Invitrogen, Carlsbad, CA). For negative control staining, the
368 primary antibody was omitted, and no staining was observed. Three 20 µm-thick coronal sections
369 at 0.4, 1.6, and 2.8 mm posterior to bregma were selected from each mouse brain for MBL-C
370 quantification. Confocal microscopy was done with a Nikon A1 confocal scan unit with a 20x 0.5
371 numerical aperture (NA) objective, managed by NIS elements software. Tissues were imaged at

372 laser excitation of 405 (for nuclei) and 647 (for MBL-C)[53]. Image acquisition was done at 12-bit,
373 keeping the fluorescent signal in a non-saturated range (0-1000 greyscale values). The
374 acquisition was done over an area sized 2x2.5 mm, positioned in the ipsilateral hemisphere along
375 the cortical region proximal to the lesion, with a pixel size of 0.62 µm. Acquisition was done over
376 8.3 µm thick stacks, with a step size of 2.075 µm. The different focal planes were merged into a
377 single stack by maximum intensity projection to ensure consistent focus throughout the sample.
378 Immunostaining for MBL-C was quantified by assessing fluorescence intensity using Fiji software.
379 To subtract the background signal, a minimum threshold was applied based in the highest
380 grayscale value of background[37]. MBL-C signal was reported as fluorescence integrated density.
381
382 **Lectin Pathway activity assay**
383 Lectin Pathway activation was quantified using the C4 cleavage assay developed by Petersen *et*
384 *al.*[54]. Nunc MaxiSorb microtiter plates were coated with 100 µl of mannan in coating buffer. After
385 overnight incubation, wells were blocked with 0.1% human serum albumin (HSA) in TBS (10mM
386 Tris-Cl, 140 mM NaCl, pH 7.4), then washed with TBS containing 0.05% Tween 20 and 5 mM
387 $CaCl_2$ (wash buffer). Plasma samples were diluted in 20 mM Tris-Cl, 1 M NaCl, 10 mM $CaCl_2$,
388 0.05% Triton X-100, 0.1% HSA, pH 7.4, which prevents activation of endogenous C4. The diluted
389 samples were added to the plate and incubated overnight at 4°C. The next day, the plates were
390 washed thoroughly with wash buffer, then 0.1 µg of purified human C4[55] in 100 µl of 4 mM
391 barbital, 145 mM NaCl, 2 mM $CaCl_2$, 1 mM $MgCl_2$, pH 7.4, was added to each well. After 1.5 h at
392 37°C, the plates were washed again, and C4b deposition was detected using alkaline
393 phosphatase-conjugated chicken anti-human C4c (Immunsystem) and the colorimetric substrate
394 pNPP.
395
396 **Experimental design and statistics**
397 Mice were randomly allocated to surgery and assigned across cages and days. To minimize
398 variability, all surgeries were performed by the same investigator. Subsequent behavioural,

histological, immunohistological, and biochemical evaluations were performed blind by another investigator. Group size is of 14 defined by the formula: $n=2\sigma^2 f(\alpha, \beta)/\Delta^2$ (SD in groups=σ, type 1 error α=0.02, type II error β=0.2, percentage difference between groups Δ=20). Standard deviation to be used in the formula for each assessment was calculated based on previous experiments with same outcome measures (e.g. behavioural deficits), resulting in σ=16.9 and n=14.4. To limit the use of animals, a *post hoc* power analysis test was done at n=7 on raw data for each experimental branch. The experiment was interrupted at n=7 for MBL-$C^{-/-}$ and MBL-$A^{-/-}$ mice since it was unable to provide significant differences using a reasonable number of animals (Δ= 3.89, σ= 22.49, thus expected n= 668.37). For MASP-$2^{-/-}$ mice the experiment was interrupted at n=7 since a significant difference was already in place due to a strong protective effect (Δ= 17.76 (3 week) Δ=19.4 (4 week)).

Groups were compared by analysis of variance and *post hoc* testing as indicated in each figure legend. A parametric or nonparametric test was selected after the Kolmogorov–Smirnov test for normality to assess whether the data for the groups were normally distributed. The constancy of the variances was checked by the Bartlett test.

A health score was obtained by stratifying the neuroscore and beam walk data sets for WT mice into four groups according to quartiles[23]. Each quartile was attributed a score ranging from 4 (good outcome) to 1 (bad outcome). The total score was the sum of the weighted scores of the two parameters, e.g., the neuroscore accounted for 50% and beam walk accounted for 50% of the final score. The effect size (odds ratio) was calculated by a Chi-square test using the Woolf logit interval for computing the 95% confidence interval, stratifying mice in terms of good outcome (defined as a score ≥3) vs. bad outcome (score < 3). Odds ratios are reported with a forest plot. Statistical analysis was performed with the standard software package GraphPad Prism (GraphPad Software Inc., San Diego, CA, USA, version 7.0); p values lower than 0.05 were considered significant.

Data Availability

The data sets generated and/or analyzed during the current study are available in the Figshare repository, 10.6084/m9.figshare.12416597.

References

1. Greig, N. H. *et al.* Incretin mimetics as pharmacologic tools to elucidate and as a new drug strategy to treat traumatic brain injury. *Alzheimers Dement.* **10**, S62–S75 (2014).
2. LaPlaca, M. C., Simon, C. M., Prado, G. R. & Cullen, D. K. CNS injury biomechanics and experimental models. in *Progress in Brain Research* (eds. Weber, J. T. & Maas, A. I. R.) vol. 161 13–26 (Elsevier, 2007).
3. Cheng, G., Kong, R., Zhang, L. & Zhang, J. Mitochondria in traumatic brain injury and mitochondrial-targeted multipotential therapeutic strategies. *Br. J. Pharmacol.* **167**, 699–719 (2012).
4. McIntosh, T. K., Juhler, M. & Wieloch, T. Novel Pharmacologic Strategies in the Treatment of Experimental Traumatic Brain Injury: 1998. *J. Neurotrauma* **15**, 731–769 (1998).
5. Simon, D. W. *et al.* The far-reaching scope of neuroinflammation after traumatic brain injury. *Nat. Rev. Neurol.* **13**, 171–191 (2017).
6. Temkin, N. R. *et al.* Magnesium sulfate for neuroprotection after traumatic brain injury: a randomised controlled trial. *Lancet Neurol.* **6**, 29–38 (2007).
7. Bains, M. & Hall, E. D. Antioxidant therapies in traumatic brain and spinal cord injury. *Biochim. Biophys. Acta BBA - Mol. Basis Dis.* **1822**, 675–684 (2012).
8. Das, M., Royer, T. V. & Leff, L. G. Interactions between aquatic bacteria and an aquatic hyphomycete on decomposing maple leaves. *Fungal Ecol.* **5**, 236–244 (2012).

9. Maas, A. I., Stocchetti, N. & Bullock, R. Moderate and severe traumatic brain injury in adults. *Lancet Neurol.* **7**, 728–741 (2008).
10. Bellander, B.-M., Singhrao, S. K., Ohlsson, M., Mattsson, P. & Svensson, M. Complement Activation in the Human Brain after Traumatic Head Injury. *J. Neurotrauma* **18**, 1295–1311 (2001).
11. Stahel, P. F. Intrathecal Levels of Complement-Derived Soluble Membrane Attack Complex (sC5b-9) Correlate with Blood–Brain Barrier Dysfunction in Patients with Traumatic Brain Injury | *Journal of Neurotrauma.* https://www.liebertpub.com/doi/abs/10.1089/089771501316919139.
12. Leinhase, I. *et al.* Pharmacological complement inhibition at the C3 convertase level promotes neuronal survival, neuroprotective intracerebral gene expression, and neurological outcome after traumatic brain injury. *Exp. Neurol.* **199**, 454–464 (2006).
13. Stahel, P. F. *et al.* Absence of the complement regulatory molecule CD59a leads to exacerbated neuropathology after traumatic brain injury in mice. *J. Neuroinflammation* **6**, 2 (2009).
14. Burk, A.-M. *et al.* Early Complementopathy After Multiple Injuries in Humans. *Shock* **37**, 348–354 (2012).
15. Orsini, F., De Blasio, D., Zangari, R., Zanier, E. R. & De Simoni, M.-G. Versatility of the complement system in neuroinflammation, neurodegeneration and brain homeostasis. *Front. Cell. Neurosci.* **8**, (2014).
16. Neglia, L. *et al.* Mannose-binding lectin has a direct deleterious effect on ischemic brain microvascular endothelial cells. *J. Cereb. Blood Flow Metab.* 0271678X19874509 (2019) doi:10.1177/0271678X19874509.

17. Dobó, J., Pál, G., Cervenak, L. & Gál, P. The emerging roles of mannose-binding lectin-associated serine proteases (MASPs) in the lectin pathway of complement and beyond. *Immunol. Rev.* **274**, 98–111 (2016).
18. Schwaeble, W. J. *et al.* Targeting of mannan-binding lectin-associated serine protease-2 confers protection from myocardial and gastrointestinal ischemia/reperfusion injury. *Proc. Natl. Acad. Sci.* **108**, 7523–7528 (2011).
19. Hayashi, M. *et al.* Cutting Edge: Role of MASP-3 in the Physiological Activation of Factor D of the Alternative Complement Pathway. *J. Immunol.* **203**, 1411–1416 (2019).
20. Hadders, M. A. *et al.* Assembly and Regulation of the Membrane Attack Complex Based on Structures of C5b6 and sC5b9. *Cell Rep.* **1**, 200–207 (2012).
21. Orsini, F. Targeting Mannose-Binding Lectin Confers Long-Lasting Protection With a Surprisingly Wide Therapeutic Window in Cerebral Ischemia | *Circulation*. https://www.ahajournals.org/doi/full/10.1161/CIRCULATIONAHA.112.103051?url_ver=Z39.88-2003&rfr_id=ori%3Arid%3Acrossref.org&rfr_dat=cr_pub++0pubmed&.
22. Orsini, F. *et al.* Mannan binding lectin-associated serine protease-2 (MASP-2) critically contributes to post-ischemic brain injury independent of MASP-1. *J. Neuroinflammation* **13**, 213 (2016).
23. Neglia, L., Oggioni, M., Mercurio, D., De Simoni, M.-G. & Fumagalli, S. Specific contribution of mannose-binding lectin murine isoforms to brain ischemia/reperfusion injury. *Cell. Mol. Immunol.* **17**, 218–226 (2020).
24. Orsini, F. Mannose-Binding Lectin Drives Platelet Inflammatory Phenotype and Vascular Damage After Cerebral Ischemia in Mice via IL (Interleukin)-1α | *Arteriosclerosis, Thrombosis, and Vascular Biology*. https://www.ahajournals.org/doi/full/10.1161/ATVBAHA.118.311058?url_ver=Z39.88-2003&rfr_id=ori:rid:crossref.org&rfr_dat=cr_pub%20%200pubmed.

25. Zanier, E. R., Fumagalli, S., Perego, C., Pischiutta, F. & De Simoni, M.-G. Shape descriptors of the “never resting” microglia in three different acute brain injury models in mice. *Intensive Care Med. Exp.* **3**, 7 (2015).
26. De Blasio, D. *et al.* Human brain trauma severity is associated with lectin complement pathway activation. *J. Cereb. Blood Flow Metab.* **39**, 794–807 (2019).
27. Longhi, L. *et al.* Mannose-Binding Lectin Is Expressed After Clinical and Experimental Traumatic Brain Injury and Its Deletion Is Protective*. *Read Online Crit. Care Med. Soc. Crit. Care Med.* **42**, 1910–1918 (2014).
28. Ali, Y. M. *et al.* The Lectin Pathway of Complement Activation Is a Critical Component of the Innate Immune Response to Pneumococcal Infection. *PLOS Pathog.* **8**, e1002793 (2012).
29. Vang Petersen, S., Thiel, S. & Jensenius, J. C. The mannan-binding lectin pathway of complement activation: biology and disease association. *Mol. Immunol.* **38**, 133–149 (2001).
30. Wallis, R., Mitchell, D. A., Schmid, R., Schwaeble, W. J. & Keeble, A. H. Paths reunited: Initiation of the classical and lectin pathways of complement activation. *Immunobiology* **215**, 1–11 (2010).
31. Chen, C.-B. & Wallis, R. Two Mechanisms for Mannose-binding Protein Modulation of the Activity of Its Associated Serine Proteases. *J. Biol. Chem.* **279**, 26058–26065 (2004).
32. Héja, D. *et al.* Monospecific Inhibitors Show That Both Mannan-binding Lectin-associated Serine Protease-1 (MASP-1) and -2 Are Essential for Lectin Pathway Activation and Reveal Structural Plasticity of MASP-2. *J. Biol. Chem.* **287**, 20290–20300 (2012).
33. Héja, D. *et al.* Revised mechanism of complement lectin-pathway activation revealing the role of serine protease MASP-1 as the exclusive activator of MASP-2. *Proc. Natl. Acad. Sci.* **109**, 10498–10503 (2012).
34. Kocsis, A. *et al.* Selective Inhibition of the Lectin Pathway of Complement with Phage Display Selected Peptides against Mannose-Binding Lectin-Associated Serine Protease

(MASP)-1 and -2: Significant Contribution of MASP-1 to Lectin Pathway Activation. *J. Immunol.* **185**, 4169–4178 (2010).

35. Degn, S. E. *et al.* Complement activation by ligand-driven juxtaposition of discrete pattern recognition complexes. *Proc. Natl. Acad. Sci.* **111**, 13445–13450 (2014).
36. Yaseen, S. *et al.* Lectin pathway effector enzyme mannan-binding lectin-associated serine protease-2 can activate native complement C3 in absence of C4 and/or C2. *FASEB J.* **31**, 2210–2219 (2017).
37. De Blasio, D. *et al.* Pharmacological inhibition of mannose-binding lectin ameliorates neurobehavioral dysfunction following experimental traumatic brain injury. *J. Cereb. Blood Flow Metab.* **37**, 938–950 (2017).
38. Pol, P. van der *et al.* Mannan-Binding Lectin Mediates Renal Ischemia/Reperfusion Injury Independent of Complement Activation. *Am. J. Transplant.* **12**, 877–887 (2012).
39. Gesuete, R. Recombinant C1 inhibitor in brain ischemic injury - Gesuete - 2009 - *Annals of Neurology - Wiley Online Library*. https://onlinelibrary.wiley.com/doi/abs/10.1002/ana.21740.
40. Dantzer, R. Cytokine-Induced Sickness Behavior: Where Do We Stand? *Brain. Behav. Immun.* **15**, 7–24 (2001).
41. Bodnar, C. N. Depression following a traumatic brain injury: uncovering cytokine dysregulation as a pathogenic mechanism Bodnar CN, Morganti JM, Bachstetter AD - *Neural Regen Res*. http://www.nrronline.org/article.asp?issn=1673-5374;year=2018;volume=13;issue=10;spage=1693;epage=1704;aulast=Bodnar.
42. Osthoff, M., Walder, B., Delhumeau, C., Trendelenburg, M. & Turck, N. Association of Lectin Pathway Protein Levels and Genetic Variants Early after Injury with Outcomes after Severe Traumatic Brain Injury: A Prospective Cohort Study. *J. Neurotrauma* **34**, 2560–2566 (2017).

43. Alawieh, A. Identifying the Role of Complement in Triggering Neuroinflammation after Traumatic Brain Injury | *Journal of Neuroscience.* https://www.jneurosci.org/content/38/10/2519.long.
44. Lynch, N. J. *et al.* Composition of the Lectin Pathway of Complement in Gallus gallus: Absence of Mannan-Binding Lectin-Associated Serine Protease-1 in Birds. *J. Immunol.* **174**, 4998–5006 (2005).
45. Pischiutta, F. *et al.* Immunosuppression does not affect human bone marrow mesenchymal stromal cell efficacy after transplantation in traumatized mice brain. *Neuropharmacology* **79**, 119–126 (2014).
46. Zanier, E. R. Human umbilical cord blood mesenchymal stem cells protect mice brain after trauma.: Read Online: *Critical Care Medicine* | Society of Critical Care Medicine. https://journals.lww.com/ccmjournal/Abstract/2011/11000/Human_umbilical_cord_blood_mesenchymal_stem_cells.17.aspx.
47. Zanier, E. R. *et al.* Bone Marrow Mesenchymal Stromal Cells Drive Protective M2 Microglia Polarization After Brain Trauma. *Neurotherapeutics* **11**, 679–695 (2014).
48. Zanier, E. R. *et al.* Fractalkine Receptor Deficiency Is Associated with Early Protection but Late Worsening of Outcome following Brain Trauma in Mice. *J. Neurotrauma* **33**, 1060–1072 (2015).
49. Brody, D. L. *et al.* Electromagnetic Controlled Cortical Impact Device for Precise, Graded Experimental Traumatic Brain Injury. *J. Neurotrauma* **24**, 657–673 (2007).
50. Mouzon, B. C. *et al.* Chronic neuropathological and neurobehavioral changes in a repetitive mild traumatic brain injury model. *Ann. Neurol.* **75**, 241–254 (2014).
51. Longhi, L. C1-inhibitor attenuates neurobehavioral deficits and reduces contusion volume after controlled cortical impact brain injury in mice*. *Crit. Care Med.*

52. Perego, C., Fumagalli, S. & De Simoni, M.-G. Temporal pattern of expression and colocalization of microglia/macrophage phenotype markers following brain ischemic injury in mice. *J. Neuroinflammation* **8**, 174 (2011).
53. Fumagalli, S. *et al.* The phagocytic state of brain myeloid cells after ischemia revealed by superresolution structured illumination microscopy. *J. Neuroinflammation* **16**, 9 (2019).
54. Petersen, S. V., Thiel, S., Jensen, L., Steffensen, R. & Jensenius, J. C. An assay for the mannan-binding lectin pathway of complement activation. *J. Immunol. Methods* **257**, 107–116 (2001).
55. Dodds, A. W. [3] Small-scale preparation of complement components C3 and C4. in *Methods in Enzymology* vol. 223 46–61 (Academic Press, 1993).

Acknowledgments

This work was supported by ERA-NET-NEURON, JTC 2016: LEAP, NEURON9-FP-044 with the following national co-found institutions: Italian Ministry of Health (*Ministero della Salute*), Italy and Medical Research Council, UK. WS, RW and SR were supported by Grant MR/R002983/1 from the Medical Research Council UK.

Author Contributions

MD conducted the experiments, acquired and analyzed the data, drafted the ms; OG, MD, IS, PC conducted the experiments, acquired and analyzed the data; FS contributed to experimental design, analyzed the data and provided critical discussion of the ms; LNJ, RS and WR provided the knock out mice, conducted the histological analysis and analyzed the data; SW provided critical review of the ms and expertise on the lectin pathway; DSMG conceived and designed the study, supervised the study, analyzed the data, wrote the ms.

Competing Interests statement

WS is a shareholder of Omeros Corp. The remaining authors declared no potential conflicts of interest with respect to the research, authorship, and/or publication of this article

Figures and Tables

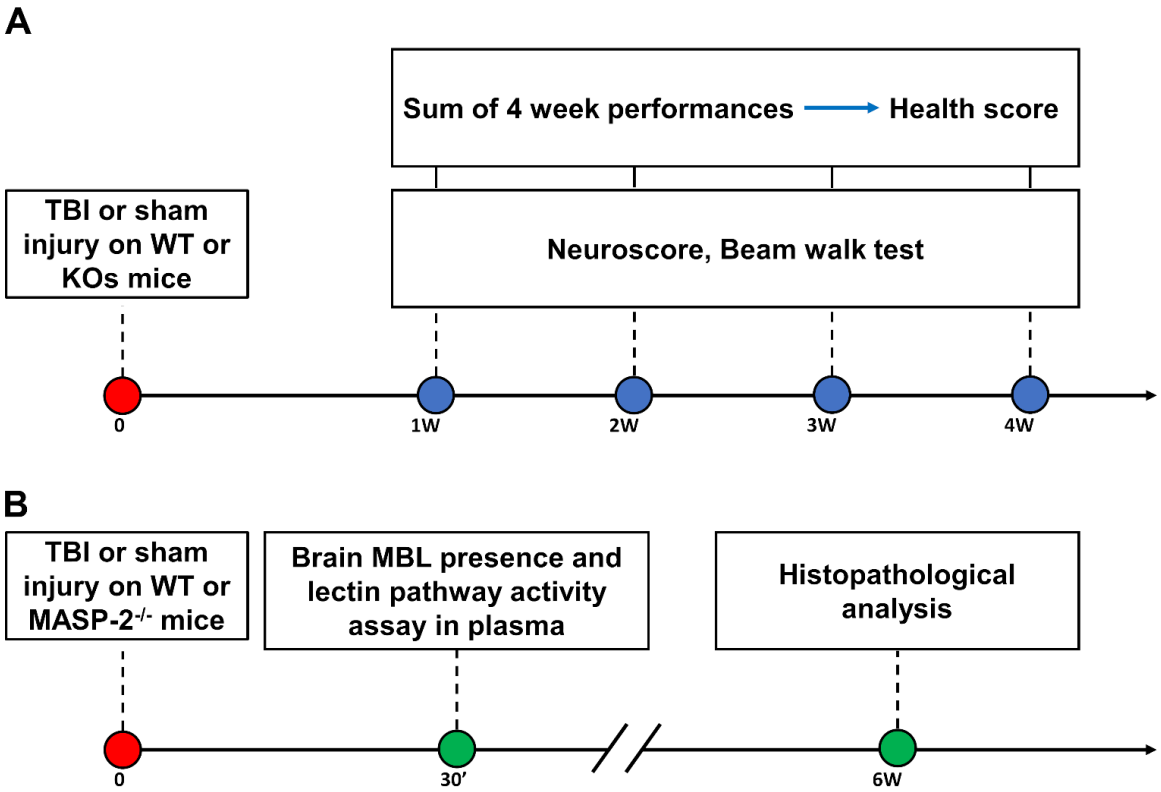

Figure 1. Experimental design.

A) WT or KOs mice (including: MASP-2$^{-/-}$, MBL$^{-/-}$, FCN-A$^{-/-}$, CL-11$^{-/-}$, MBL-C$^{-/-}$, MASP-1/3$^{-/-}$ and MBL-A$^{-/-}$) were subjected to TBI or sham injury. Sensorimotor deficits were assessed weekly by neuroscore and beam walk test. The sum of 4-week performances of each mouse genotype has been used to calculate the health score. **B)** MBL brain presence and residual LP activity in plasma was assed in MASP-2$^{-/-}$ and WT TBI mice 30' after surgery. Histopathological analysis was done for MASP-2$^{-/-}$ and WT mice at 6 weeks after TBI.

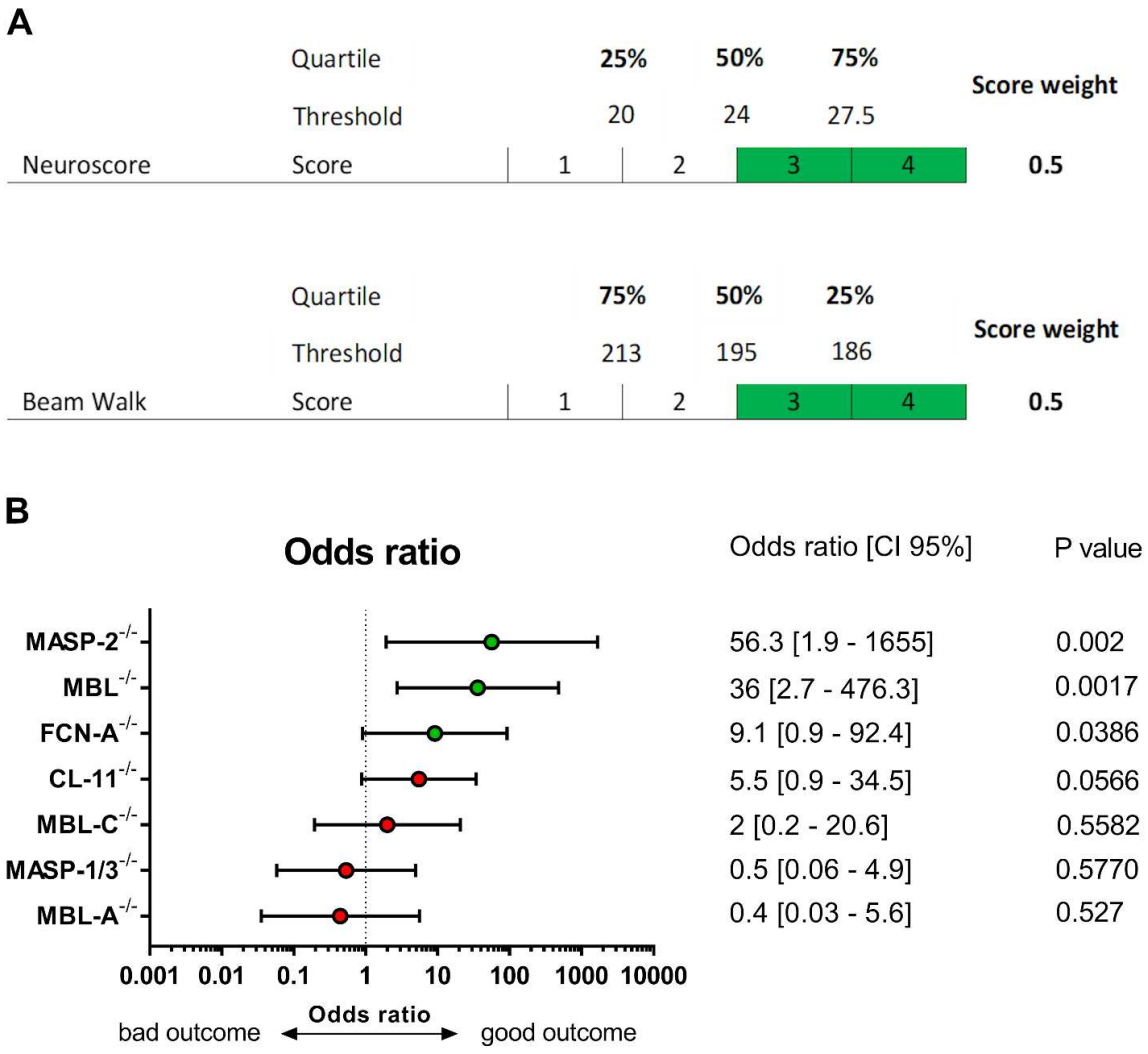

Figure 2. Association of LP protein deficiency with the behavioral outcome of traumatized mice over 4 weeks.

A) The health score was obtained by rating mice from 4 (good outcome) to 1 (bad outcome) based on quartiles of the neuroscore and beam walk values over the 4 weeks of observation. The final score was the sum of the weighted scores of the two parameters, e.g. the neuroscore and beam walk each accounted for 50% of the final score. **B)** Association (odds ratio; 95% confidence interval) between the genotype and health score. The odds ratio was calculated by a Chi-square test using the Woolf logit interval for calculating the 95% confidence interval (CI 95%), stratifying

mice in terms of good outcome (defined as a score ≥ 3) vs. bad outcome (score < 3). MASP-2$^{-/-}$, MBL$^{-/-}$ and FCN-A$^{-/-}$ mice were significantly associated with good outcome scores.

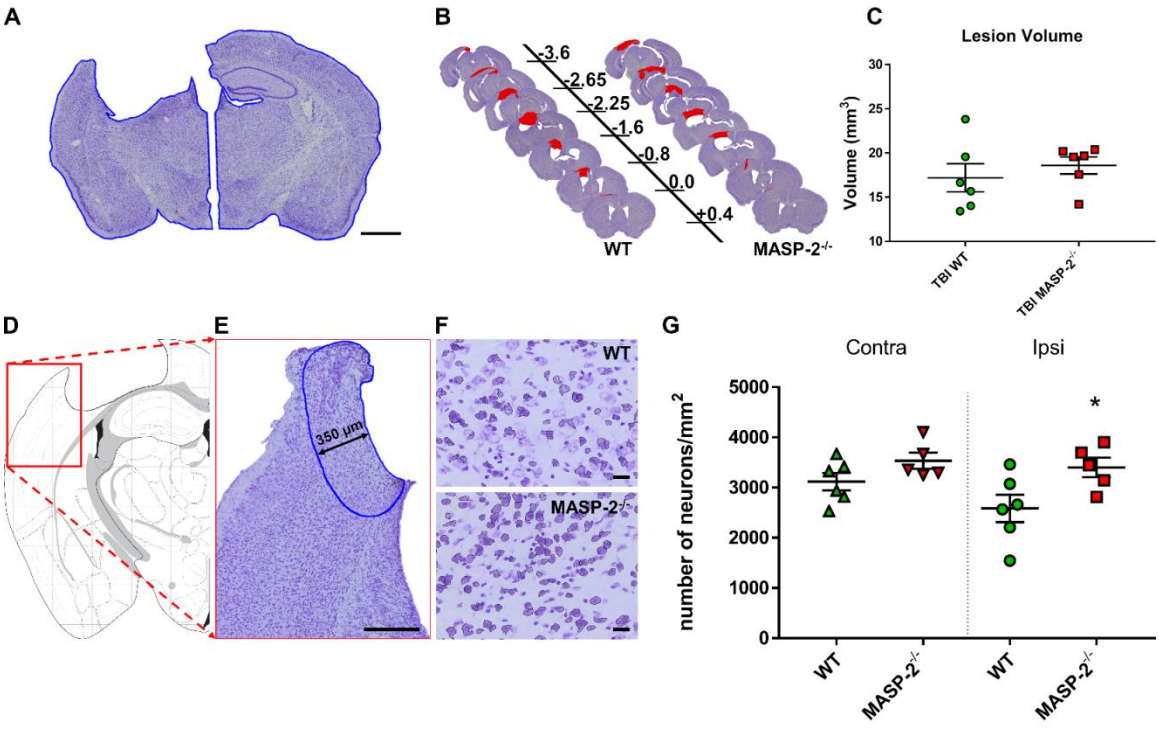

Figure 3. Histological analysis of lesion at six weeks after TBI in WT and MASP-2$^{-/-}$ mice.

A) Representative image of Cresyl violet staining in ipsilateral and contralateral hemisphere. The lesion volume was evaluated based on the different extents of the ipsilateral and contralateral hemispheres, outlined in blue. Scale bar 1 mm. **B)** Representative images of quantified sections for lesion volume at six weeks after TBI in WT and MASP-2$^{-/-}$ mice. Distance from bregma in mm is indicated. **C)** Quantification of the lesion showed no differences between WT and MASP-2$^{-/-}$ mice six weeks after TBI. The data is shown as a scatter dot plot, line at mean ± SEM (n = 6); Mann-Whitney test. **D)** Anatomical location of area of interest (red box). **E**) Positioning of the cortical region of interest (blue outline) for calculating neuronal cell viability, traced at a distance of 350 µm from the contusion edge. Scale bar 350 µm. **F)** 20x high magnified fields of view showing a higher presence of neurons in MASP-2$^{-/-}$ than WT mice. Scale bars 20 µm. **G)** Quantification of neuronal density in the region of interest. MASP-2$^{-/-}$ mice had higher neuronal density in the ipsilateral cortex than WT mice. The data is shown as a scatter dot plot, line at

636 mean ± SEM (n = 5-6); Two-way Anova followed by Sidak's post hoc test, *p <0.05 compared

637 with ipsi WT.

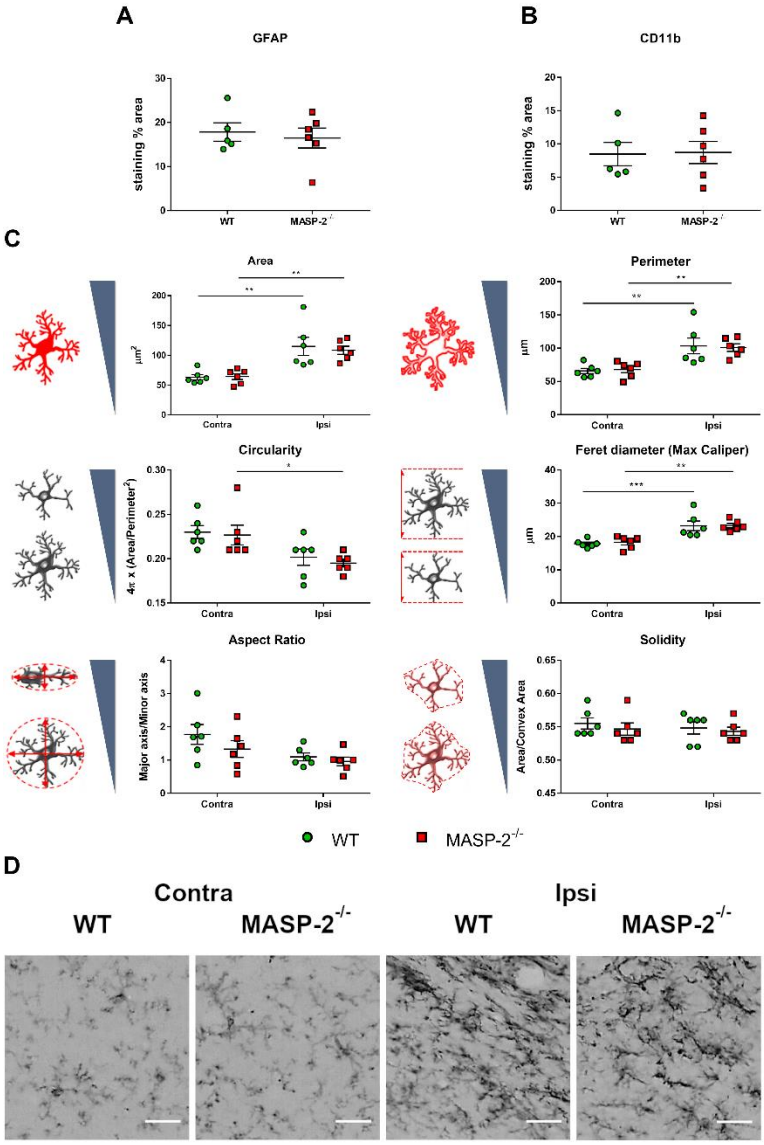

652

653 **Figure 4. Inflammation markers and shape descriptors for microglia six weeks after TBI in**

654 **WT and MASP-2$^{-/-}$ mice.**

655

656 **A, B)** MASP-2 deletion did not affect the level of inflammatory markers such as glial fibrillary

657 acidic protein (GFAP) and CD11b. The data is shown as a scatter dot plot, line at mean ± SEM (*n*

658 = 5-6); unpaired t-test. **C)** Shape descriptors of CD11b positive cells showed that at six weeks

659 after TBI microglia are still activated, having increased area, perimeter, Feret diameter and

ramifications (indicated by lower circularity) higher in ipsi than in contralateral side. The drawings beside the y-axis indicate the expected values for each parameter depending on cell shape o symmetry. Microglia morphology did not differ between the two genotypes. The data is shown as a scatter dot plot, line at mean ± SEM (*n* = 6); Two-way Anova followed by Sidak's post hoc test **D)** Representative high-magnification images of CD11b positive cells showing activated microglia in the ipsilateral side of both WT and MASP-2$^{-/-}$ TBI mice, scale bar 20 µm.

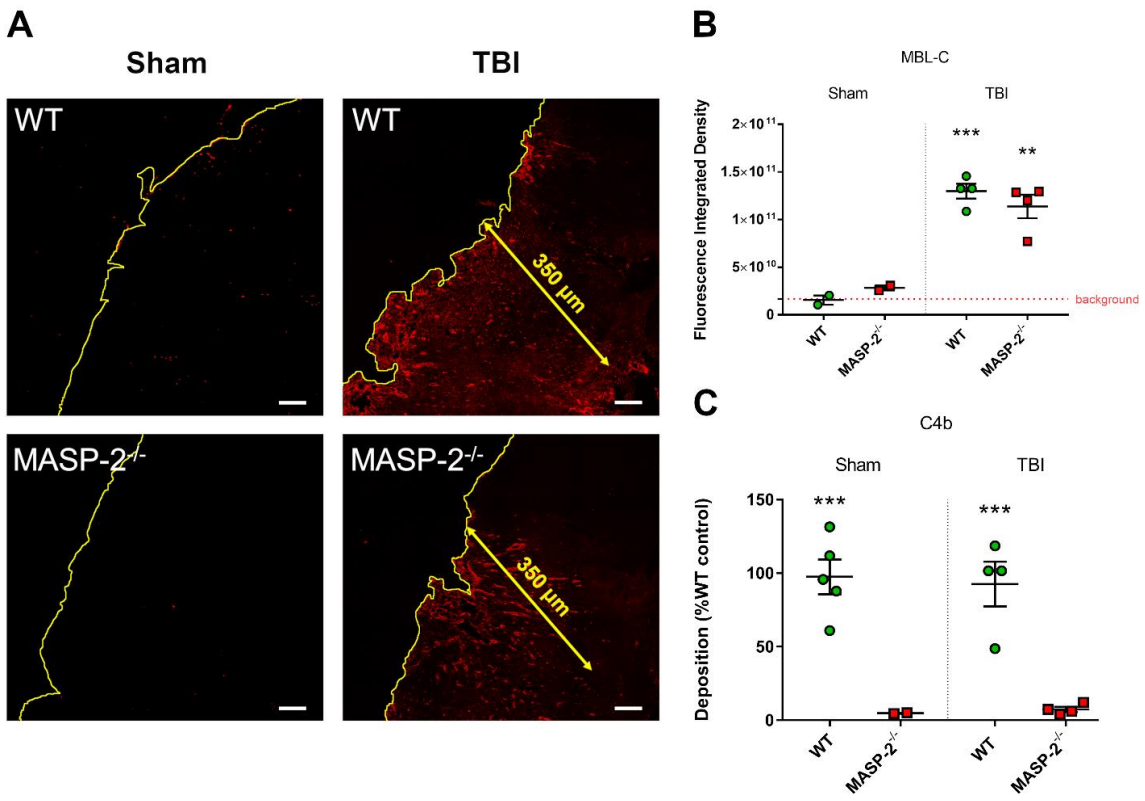

Figure 5. MBL-C deposition in the brain and LP activation in plasma 30 minutes after TBI in WT or MASP-2$^{-/-}$ mice.

A) Representative low-magnification images of MBL-C immunolabeling at 30 minutes after TBI or sham surgery (the cortical edge is outlined in yellow). MBL-C quantification was done over an area of 350 µm from the contusion edge (Fig. 2). Scale bars 50 µm. **B**) MBL-C deposition in brains of MASP-2$^{-/-}$ mice was similar to that of WT. Data is shown as a scatter dot plot, line at mean ± SEM (n = 2-4). Two-way Anova followed by Sidak's post hoc test, $^{**}p < 0.01$ compared with Sham MASP-2$^{-/-}$, $^{***}p < 0.001$ compared with Sham WT. **C**) In vitro assay for LP activation on mannans – driven by MBL - showed a decreased activation, indicated by the absence of C4b deposition, in plasma from MASP-2$^{-/-}$ than in WT mice. The data is shown as a scatter dot plot, line at mean ± SEM (n = 2-4), Two-way Anova followed by Sidak's post hoc test, $^{***}p < 0.001$ compared with Sham or TBI WT.

Table 1. Summary of the outcome measures in the MASP-2$^{-/-}$, MBL$^{-/-}$, FCN-A$^{-/-}$, CL-11$^{-/-}$, MBL-C$^{-/-}$, MASP-1/3$^{-/-}$ or MBL-A$^{-/-}$ TBI mice. For MBL$^{-/-}$, data were obtained from the previous paper by Longhi et al. [27]

Strain		1 week		2 week		3 week		4 week	
		% of WT	*p* value	% of WT	*p* value	% of WT	*p* value	% of WT	*p* value
MASP-2$^{-/-}$	Neuroscore	+ 11.4	0.6079	+ 4.3	0.9605	+ 13.6	0.4541	-5.9	0.8809
	Beam Walk	+ 5.5	0.9608	+ 27.9	0.0681	+ 32.1	0.0202	+ 36	0.0091
MBL$^{-/-}$	Neuroscore	+ 33.7	0.0997	+ 42.8	0.0023	+ 37.2	0.0011	+ 35.6	0.0003
	Beam Walk	+ 12.9	0.2972	+ 24.03	0.0131	+ 25.1	0.0133	+ 21.4	0.0742
FCN-A$^{-/-}$	Neuroscore	+ 19.7	0.9253	+ 0.37	>0.9999	-7.9	0.7784	+5.3	0.9171
	Beam Walk	+ 6.7	0.9253	+ 15	0.5412	+ 13	0.685	+ 9.9	0.829
CL-11$^{-/-}$	Neuroscore	+ 16	0.4086	+ 13.5	0.5552	+ 11.2	0.631	+ 11.9	0.5552
	Beam Walk	-4.9	0.8735	+ 11.1	0.3198	+ 15.8	0.0711	+ 23.5	0.0024
MBL-C$^{-/-}$	Neuroscore	+ 10	>0.9999	+ 2.9	>0.9999	+ 11.1	>0.9999	-16.7	0.8796
	Beam Walk	-3.5	>0.9999	-3.5	>0.9999	3.6	>0.9999	+ 3.9	>0.9999
MASP-1/3$^{-/-}$	Neuroscore	+ 9.1	0.9426	+ 11.9	0.784	+ 8.7	0.8759	-1.9	0.9976
	Beam Walk	+ 1.07	0.9997	+ 0.56	>0.9999	-2.6	0.997	0	>0.9999
MBL-A$^{-/-}$	Neuroscore	+ 4.5	0.9986	+ 7.1	0.989	-2.9	0.9986	-19.5	0.589
	Beam Walk	-10	0.9025	-4.2	0.9932	-9.8	0.9133	-11.01	0.8786

Figures

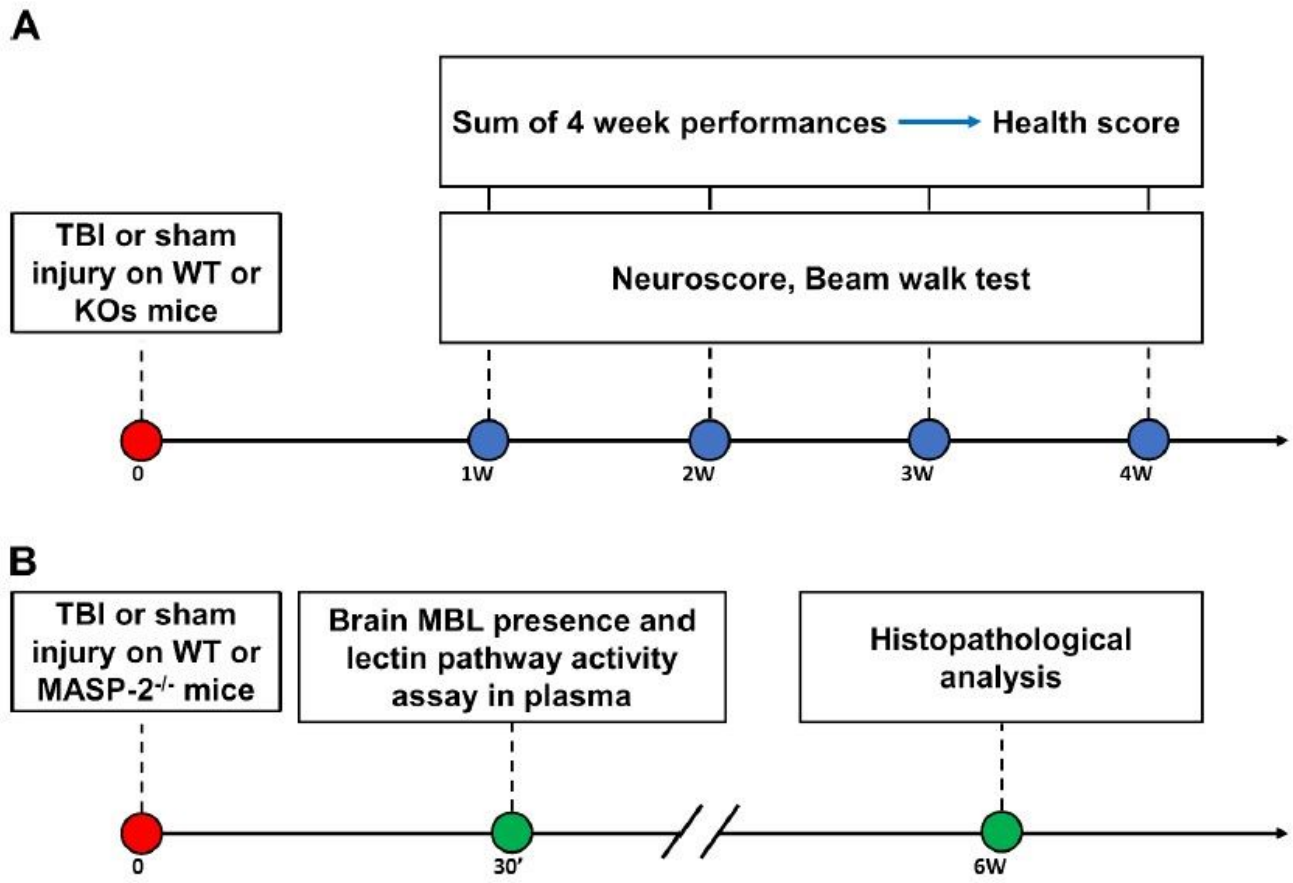

Figure 1

Experimental design. A) WT or KOs mice (including: MASP-2-/-, MBL-/-, FCN-A-/-, CL-11-/-, MBL-C-/-, MASP-1/3-/- and MBL-A-/-) were subjected to TBI or sham injury. Sensorimotor deficits were assessed weekly by neuroscore and beam walk test. The sum of 4-week performances of each mouse genotype has been used to calculate the health score. B) MBL brain presence and residual LP activity in plasma was assed in MASP-2-/- and WT TBI mice 30' after surgery. Histopathological analysis was done for MASP-2-/- and WT mice at 6 weeks after TBI.

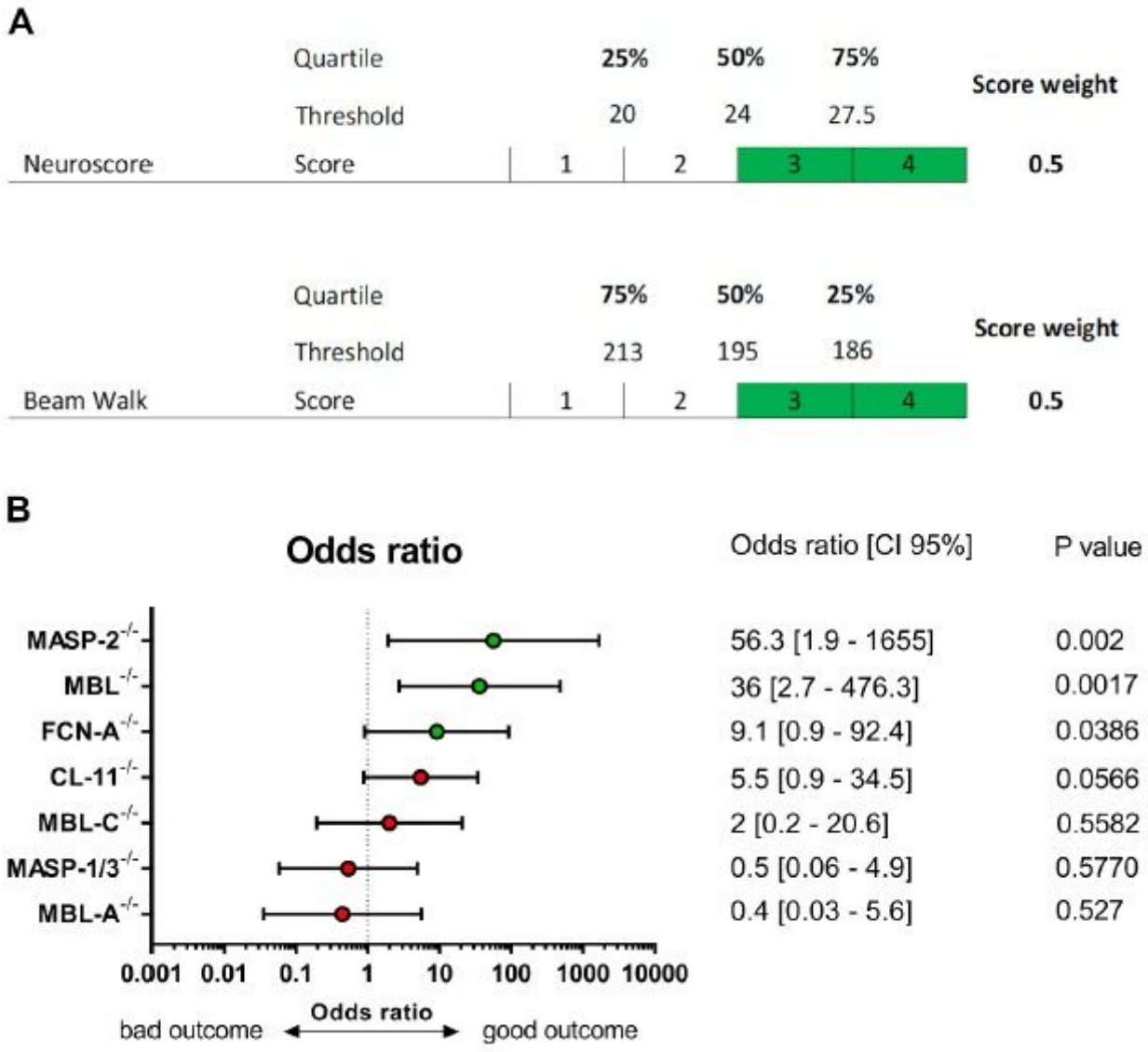

Figure 2

Association of LP protein deficiency with the behavioral outcome of traumatized mice over 4 weeks. A) The health score was obtained by rating mice from 4 (good outcome) to 1 (bad outcome) based on quartiles of the neuroscore and beam walk values over the 4 weeks of observation. The final score was the sum of the weighted scores of the two parameters, e.g. the neuroscore and beam walk each accounted for 50% of the final score. B) Association (odds ratio; 95% confidence interval) between the genotype and health score. The odds ratio was calculated by a Chi-square test using the Woolf logit interval for calculating the 95% confidence interval (CI 95%), stratifying mice in terms of good outcome (defined as a score ≥ 3) vs. bad outcome (score < 3). MASP-2-/-, MBL-/- and FCN-A-/- mice were significantly associated with good outcome scores.

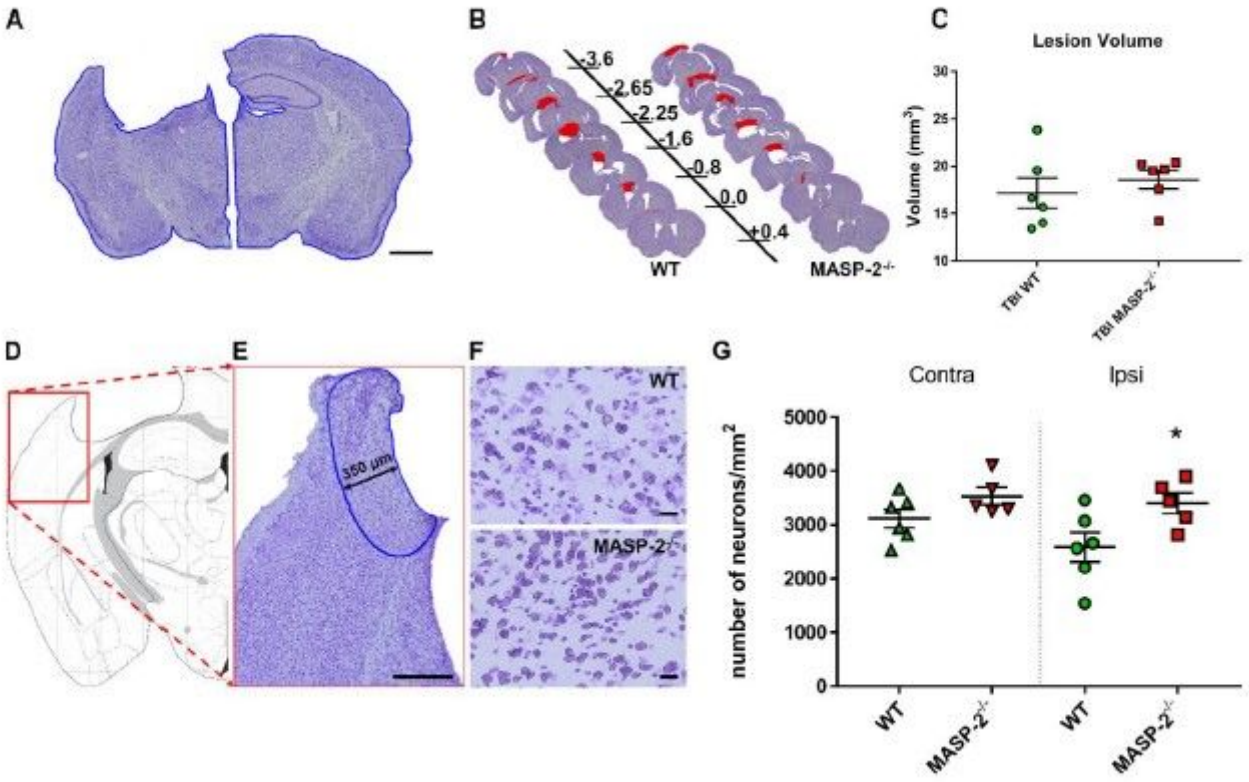

Figure 3

Histological analysis of lesion at six weeks after TBI in WT and MASP-2-/- mice. A) Representative image of Cresyl violet staining in ipsilateral and contralateral hemisphere. The lesion volume was evaluated based on the different extents of the ipsilateral and contralateral hemispheres, outlined in blue. Scale bar 1 mm. B) Representative images of quantified sections for lesion volume at six weeks after TBI in WT and MASP-2-/- mice. Distance from bregma in mm is indicated. C) Quantification of the lesion showed no differences between WT and MASP-2-/- mice six weeks after TBI. The data is shown as a scatter dot plot, line at mean ± SEM (n = 6); Mann-Whitney test. D) Anatomical location of area of interest (red box). E) Positioning of the cortical region of interest (blue outline) for calculating neuronal cell viability, traced at a distance of 350 µm from the contusion edge. Scale bar 350 µm. F) 20x high magnified fields of view showing a higher presence of neurons in MASP-2-/- than WT mice. Scale bars 20 µm. G) Quantification of neuronal density in the region of interest. MASP-2-/- mice had higher neuronal density in the ipsilateral cortex than WT mice. The data is shown as a scatter dot plot, line at mean ± SEM (n = 5-6); Two-way Anova followed by Sidak's post hoc test, *p <0.05 compared with ipsi WT.

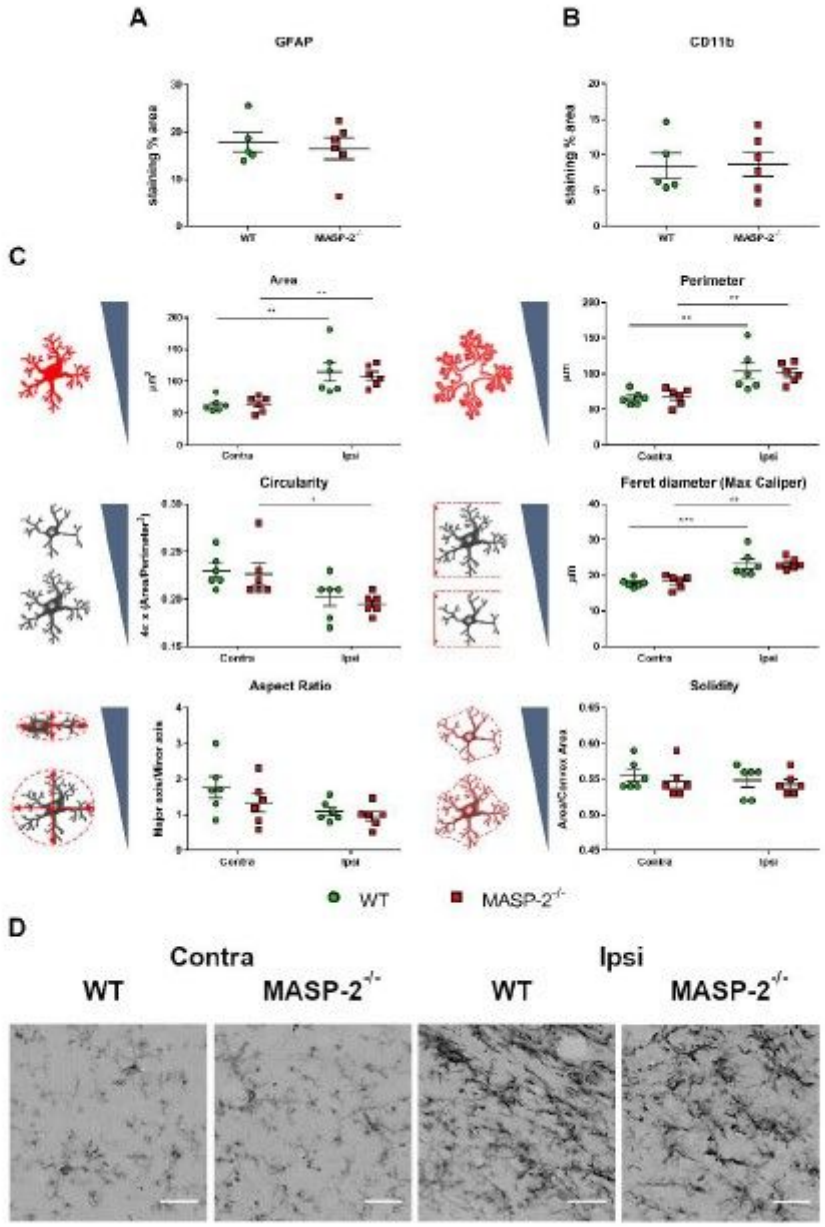

Figure 4

Inflammation markers and shape descriptors for microglia six weeks after TBI in WT and MASP-2-/- mice. A, B) MASP-2 deletion did not affect the level of inflammatory markers such as glial fibrillary acidic protein (GFAP) and CD11b. The data is shown as a scatter dot plot, line at mean ± SEM (n = 5-6); unpaired t-test. C) Shape descriptors of CD11b positive cells showed that at six weeks after TBI microglia are still activated, having increased area, perimeter, Feret diameter and ramifications (indicated by lower circularity) higher in ipsi than in contralateral side. The drawings beside the y-axis indicate the expected values for each parameter depending on cell shape o symmetry. Microglia morphology did not differ between the two genotypes. The data is shown as a scatter dot plot, line at mean ± SEM (n = 6); Two-way Anova followed by Sidak's post hoc test D) Representative high-magnification images of CD11b positive

cells showing activated microglia in the ipsilateral side of both WT and MASP-2-/- TBI mice, scale bar 20 µm.

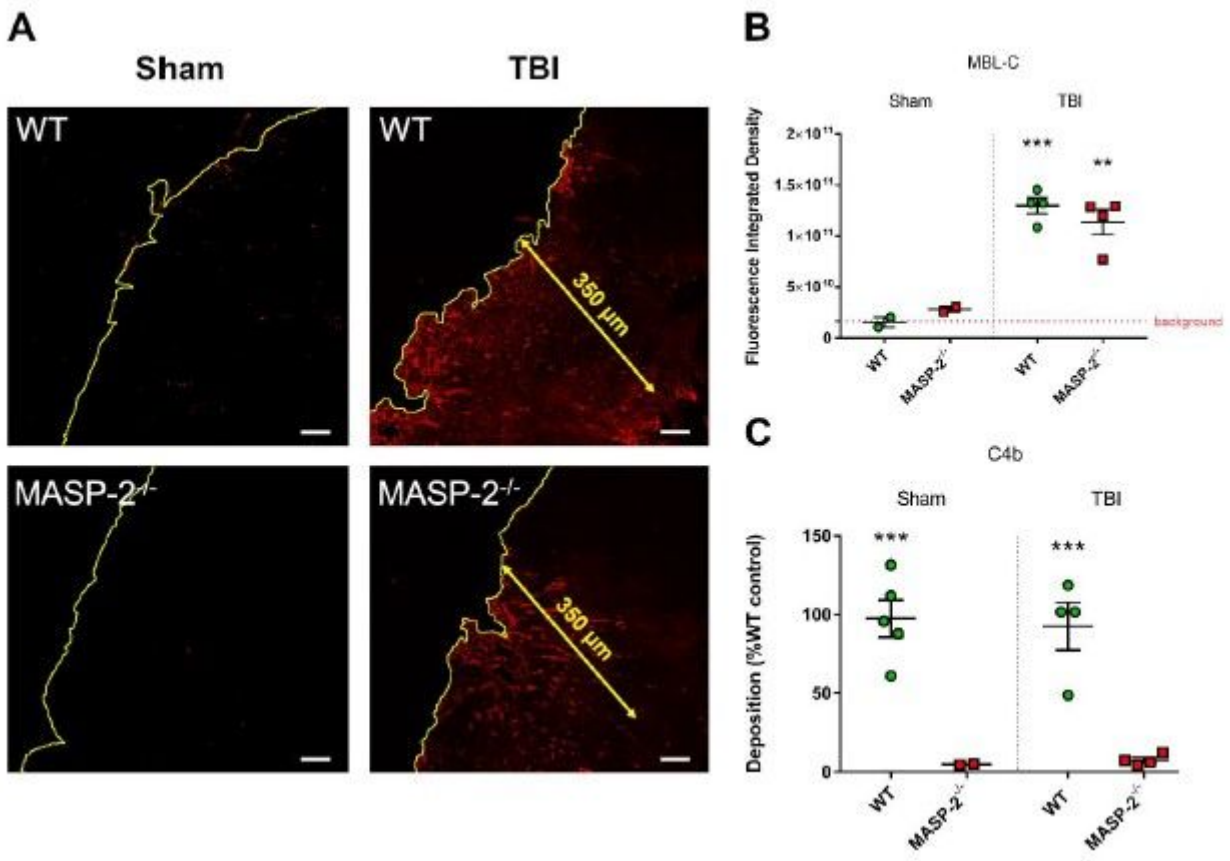

Figure 5

MBL-C deposition in the brain and LP activation in plasma 30 minutes after TBI in WT or MASP-2-/- mice. A) Representative low-magnification images of MBL-C immunolabeling at 30 minutes after TBI or sham surgery (the cortical edge is outlined in yellow). MBL-C quantification was done over an area of 350 µm from the contusion edge (Fig. 2). Scale bars 50 µm. B) MBL-C deposition in brains of MASP-2-/- mice was similar to that of WT. Data is shown as a scatter dot plot, line at mean ± SEM (n = 2-4). Two-way Anova followed by Sidak's post hoc test, **p < 0.01 compared with Sham MASP-2-/-, ***p < 0.001 compared with Sham WT. C) In vitro assay for LP activation on mannans – driven by MBL - showed a decreased activation, indicated by the absence of C4b deposition, in plasma from MASP-2-/- than in WT mice. The data is shown as a scatter dot plot, line at mean ± SEM (n = 2-4), Two-way Anova followed by Sidak's post hoc test, ***p < 0.001 compared with Sham or TBI WT.